ACS APPLIED MATERIALS & INTERFACES

Research Article

www.acsami.org

Silver Nanoparticle-Mesoporous Oxide Nanocomposite Thin Films: A Platform for Spatially Homogeneous SERS-Active Substrates with Enhanced Stability

Alejandro Wolosiuk,[†] Nicolás G. Tognalli,[‡,§] Eduardo D. Martínez,[†,∥] Mara Granada,[‡] M. Cecilia Fuertes,[†,∥] Horacio Troiani,[‡] Sara A. Bilmes,[⊥] Alejandro Fainstein,[‡] and Galo J. A. A. Soler-Illia*[,†,⊥]

[†]Gerencia Química, Centro Atómico Constituyentes, Comisión Nacional de Energía Atómica (CNEA), Av. Gral Paz 1499 B1650KNA San Martín, Buenos Aires, Argentina

[‡]Centro Atómico Bariloche, CNEA, 8400 San Carlos de Bariloche, Río Negro, Argentina

[§]Centro de Innovación Tecnológica, Empresarial y Social (CITES), S2322 Sunchales, Santa Fe, Argentina

[∥]Instituto Sabato, Universidad Nacional de San Martín, CNEA, B1650HMP, San Martin, Buenos Aires, Argentina

[⊥]DQIAyQF, FCEN, Universidad de Buenos Aires, Ciudad Universitaria, Pabellón II, C1428EHA, Buenos Aires, Argentina

Supporting Information

ABSTRACT: We introduce a nanoparticle-mesoporous oxide thin film composite (NP-MOTF) as low-cost and straightforward sensing platforms for surface-enhanced Raman Spectroscopy (SERS). Titania, zirconia, and silica mesoporous matrices templated with Pluronics F-127 were synthesized via evaporation-induced self-assembly and loaded with homogeneously dispersed Ag nanoparticles by soft reduction or photoreduction. Both methods give rise to uniform and reproducible Raman signals using 4-mercaptopyridine as a probe molecule. Details on stability and reproducibility of the Raman enhancement are discussed. Extensions in the design of these composite structures were explored including detection of nonthiolated molecules, such as rhodamine 6-G or salicylic acid, patterning techniques for locating the enhancement regions and bilayered mesoporous structures to provide additional control on the environment, and potential size-selective filtration. These inorganic oxide−metal composites stand as extremely simple, reproducible, and versatile platforms for Raman spectroscopy analysis.

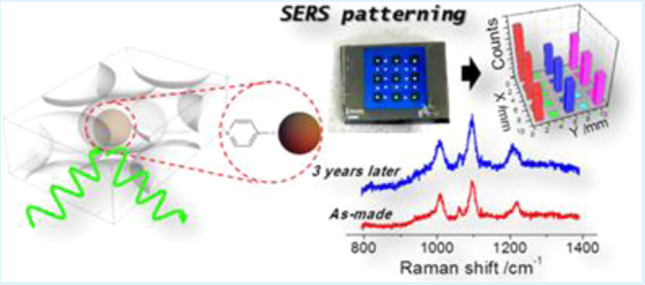

KEYWORDS: *surface-enhanced Raman spectroscopy (SERS), mesoporous thin films, silver nanoparticles, photodeposition, sensors, plasmonics*

INTRODUCTION

Enhancement of molecular Raman scattering by metallic surfaces opened an exciting research area for single molecule sensing and microscopy, adding new levels of detection not previously envisaged.[1−5] A surface-enhanced Raman scattering (SERS) signal is produced under light excitation of the surface plasmon resonance of metallic nanostructures. The electric field enhancement concentrates in the so-called "hot spots", which are found in gaps between nanoparticles (NPs) in dimers, aggregates, and large fractal structures.[6−8] In addition, certain electronic features of the adsorbed molecule are also required, although the specific mechanism of the chemical contribution to the surface enhancement remains under dispute.[9] Among the metallic surfaces where SERS is observed, silver is the metal of choice because it exhibits a higher scattering cross section which results in larger enhancements. Moreover, tailoring the shape and size of metallic nanoparticles allows a fine-tuning of the plasmon absorption which in turn contributes to the enhancement of the Raman signal.

The reproducible preparation of surfaces with a high density of active spots is one of the main current issues regarding SERS active substrates for routine analysis.[3,10] The reproducible fabrication of this kind of SERS substrates relies mostly on the use of templates that drive NP formation, deposition, or synthesis, resulting in ordered arrays of NPs and nanoobjects:[11] alumina anodized oxides membranes, lithography based nanoholes, metal electrodeposition through colloidal templates, nanosphere lithography and self-assembled 2D ordered arrays.[12−17] The designed platforms should present not only high enhancement factors but also the following issues: (i) homogeneity of the enhancement, that is, spot-to-spot

Received: January 28, 2014
Accepted: March 11, 2014
Published: March 11, 2014

   dx.doi.org/10.1021/am500631f | ACS Appl. Mater. Interfaces 2014, 6, 5263−5272

reproducibility of the Raman signal,[18] (ii) substrate-to-substrate reproducibility, (iii) high stability of the nanostructure, and (iv) easy and cost-effective preparation and use.[19] As the larger enhancements are produced in hot-spots,[6] an homogeneous distribution of them should be pursued. This is a major challenge since the typical strategies involve either the induced aggregation of Ag or Au NPs from colloidal dispersions, or the fabrication of nanostructured surfaces using high resolution nanofabrication techniques, which present cost and processing limitations for large scale production.

Nanoporous systems present an interesting and desirable feature for SERS substrates: the possibility to confer selectivity to the analytes under sensing, either by selective adsorption of molecules or by controlled diffusion across membranes. The fabrication of inexpensive, robust, and reproducible SERS active substrates with regular and highly controlled metallic nanostructures included in porous matrices fuels this research area toward real-world environment field data acquisition devices and trace analysis. Recently, several works reported the use of microporous or mesoporous frameworks loaded with metallic NPs as SERS substrates with potential molecular sieving activity.[20−23] To project these encouraging systems to real analytical applications, a broader study concerning the homogeneity, stability, reproducibility, and comparison between different materials is needed.

In this work, we present the use of mesoporous oxide thin films (MOTF) for synthesizing Ag SERS active substrates using soft reduction techniques. Titania, silica, or zirconia MOTF were synthesized by evaporation induced self assembly (EISA). The precise localization of Ag NPs within the MOTF and the degree of control of the electroless[24] or photoinduced infiltration[25] lead to the straightforward fabrication of SERS substrates. This EISA-based preparation is highly attractive because of the simple experimental setup required and the high control regarding film homogeneity, mesostructure, pore size and thickness.[26] Soft coating processes allow film deposition on a variety of surfaces: from flat substrates to complex systems such as mesoscopic lithographic channels.[27] A fully supported platform made up of metal NP-mesoporous oxide framework with controlled SERS active spots would allow connectivity, facilitating the diffusion of analytes along the supramolecular structure and preventing nanoparticle aggregation. Although recent work has reported SERS-active MOTF-based materials,[20,21] we present here a complete study that includes a thorough analysis of the signal intensity and reproducibility, and its dependence on the NP loading. The influence of particles formed on the surface, the role of the wafer material and the long-term SERS-active substrate performance of the nanocomposites are also discussed. These are essential features in the design of actual analytical applications that so far have not been addressed in this kind of materials. In addition, the method presented here merges soft reduction with lithographic patterning, opening the path to combine standard *top−down* and *bottom−up* approaches,[28] aiming at integrated architectures for advanced sensors.[29,30] We also demonstrate SERS-active multilayered mesostructures that can be potentially applied in smart perm-selective membranes,[31,32] responsive photonic stacks[33,34] and complex sorption films,[29] including hierarchical structures.[35] The patterned NP-MOTF nanocomposites in microchannel networks represent an excellent perspective for microfluidic and lab-on-chip setups.

EXPERIMENTAL SECTION

Film Synthesis. Titania, zirconia, and silica MOTF were deposited by dip-coating on glass or silicon substrates at a relative humidity (RH) of 40−50% for titania or silica and 20% for zirconia. The dip-coating speed used varied between 1 and 2 mm·s^{-1}. The detailed preparation techniques have been reported elsewhere.[36,37] $ZrCl_4$, $TiCl_4$, and $Si(OEt)_4$ were used as the inorganic precursors. Titania precursor solutions were used without aging, and the films were made at 30 °C solution temperature. The composition used was $TiCl_4$/EtOH/H_2O 1:40:10. Cetyltrimethylammonium bromide (CTAB) was used as a template of SiO_2 films, and Pluronics F127 block copolymer $(HO(CH_2CH_2O)_{106}(CH_2CH(CH_3)O)_{70}(CH_2CH_2O)_{106}OH)$, for large-pore materials.

After deposition, films were placed in 50% RH chambers for 24 h, and subjected to a stabilizing thermal treatment procedure consisting of two successive 24 h heat treatments at 60 and 130 °C, and a final 2 h step at 200 °C. The template was finally eliminated from all the layers by heating at 350 °C under a still air atmosphere in a tubular oven, leading to the formation of transparent crack-free thin films.

Ag Nanoparticle Synthesis. Synthesis of Raman active metallic centers in mesoporous oxide matrices (Ag@MOx) can be accomplished through electrochemical methods,[38,39] heat postreduction synthesis,[40,41] photochemistry,[42] or "one pot" synthesis of EISA solutions precursors and protected nanoparticles.[43] In this context, nucleation and further growth of metallic seeds are key aspects to control to obtain a 3D inverse metallic framework or a nanocomposite comprising domains of oxide and metal nanoparticles.[44] Therefore, the pore framework provides an organized array of fixed size and interconnected nanoreactors for NPs synthesis. The Ag loading of MOTFs was performed following two different procedures previously developed in our laboratory: electroless deposition[24] and photoreduction.[45] All MOTF samples, with or without Ag NPs, were stored under darkness to avoid photodegradation.

Electroless Deposition Method. Ag NPs were synthesized within mesoporous thin films as follows: first, calcined films were immersed in a 1:1 water/ethanol mixture of $AgNO_3$ 0.05 M for 15 min. Then, 7% w/w formaldehyde (HCHO) solution was added until a 1% w/w final concentration was reached and left under stirring for 2 h.[24] After 15−20 min a noticeable change in color was observed in TiO_2 and ZrO_2 mesoporous films and 6 h later, a gray silver film was wiped off from the porous substrate with a tissue paper. To obtain Ag deposition in SiO_2 films, the reducing agent concentration is higher and much longer reduction times are needed.[24] Alternatively, we employed a $SnCl_2$ 10^{-4} M/HCl 0.01 M solution for activation of the silica pores for 10 min.[46]

Photo-Reduction Method. TiO_2 mesoporous thin films deposited on silicon substrates were placed in a plastic container and covered with a 1:1 water/ethanol mixture of $AgNO_3$ 0.01 M. After ten minutes in the dark to favor the adsorption of Ag^+ cations on the pore surface, the container was placed under a UV lamp (355 nm, 15 W Phillips black light) for the desired exposure time. An acetate lithography mask was used to pattern the Ag NPs loading.[25] After the Ag infiltration synthesis, the film surface was gently cleaned with tissue paper wet with ethanol to remove any deposit formed on the surface of the films. As will be discussed later, the presence of residual Ag particles on the surface has a significant influence on the SERS performance.

Molecule Adsorption in Ag@MOTF Frameworks. 4-Mercaptopyridine (4-MP, Sigma−Aldrich, 95%), was used as received. Molecule adsorption was carried out as follows. First the NP-MOTF nanostructures were immersed in ethanol solutions of 10 μM, 50 μM or 250 μM of 4-MP during 30 min. After that, substrates were rinsed with ethanol and finally dried under a nitrogen gas flow. The same protocol was used in the case of rhodamine 6G (incubated from a 7.5 μM solution); adsorption of salicylic acid was performed from 10 mM aqueous solution at pH 6.

Raman Measurements. The enhanced Raman scattered intensity of 4-MP was measured onto Ag-loaded TiO_2, ZrO_2, or SiO_2 samples between 800 and 1300 cm^{-1} using a Jobin-Yvon T64000 triple spectrometer operating in subtractive mode and equipped with a

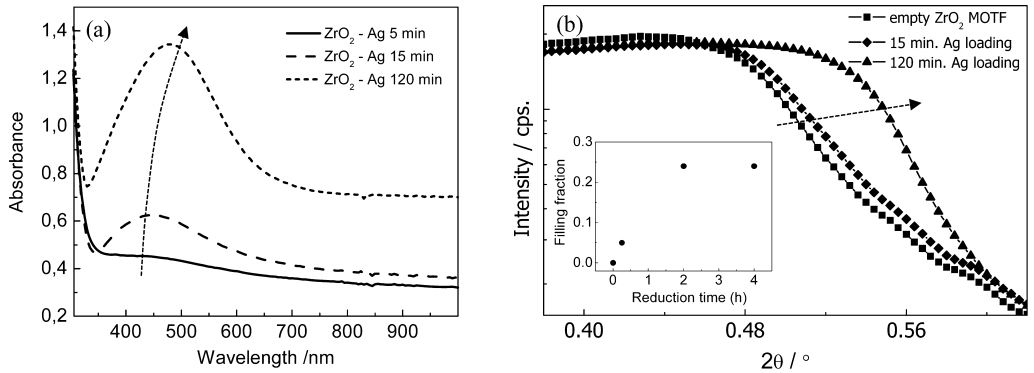

Figure 1. (a) Absorption spectra of Ag@ZrO_2−F127 composite films synthesized by electroless reduction with different reduction times. The blue arrow indicates the evolution of the plasmon resonance. (b) XRR curves for Ag@ZrO_2−F127 with different electroless reduction times. The arrow indicates increasing time. Inset: Time evolution of the pore filling fraction with Ag NP, calculated from XRR critical angle.

liquid-N_2 cooled charge coupled device. The excitation was performed with an Ar−Kr ion laser using energies between 1.834 eV (676 nm) and 2.707 eV (458 nm). Typical powers were around 10 mW, concentrated on either a ∼100 μm diameter circular spot, or a 7 mm long and ∼100 μm wide line focus. These were chosen to reduce the photon-induced degradation of the samples. Under the worst situation (circular spot) the photobleaching was determined to be around 5% after 120 s of data acquisition (Supporting Information, Figure S1).

Film Characterization. *Small Angle X-ray Scattering (SAXS) and X-ray Reflectometry (XRR).* Film mesostructures were analyzed using Small Angle X-ray Scattering (SAXS) at the D11A-SAXS2 line of LNLS (λ = 1.608 or 1.488 Å) at normal and 3° incidence and a MARCCD 2D detector. Films thickness and density were obtained from X-ray reflectometry (XRR) measurements performed at the D10A-XRD2 line of Laboratório Nacional de Luz Síncrotron, Campinas, SP, Brazil (λ = 1.5498 Å). To obtain accurate film density values, the critical angle measurements were performed at low humidity, to avoid atmospheric water condensation within the pores that leads to underestimation of mesoporosity. Data and model analysis is described in a previous work.[24]

Electron Micoscopy (TEM and SEM). TEM images were obtained from a CM 200 Philips high-resolution transmission electron microscope equipped with an ultra twin objective lens and an acceleration voltage of 200 kV (CAB−CNEA). Samples were obtained by scratching the Ag@MOTF films from the substrate and deposited on carbon coated copper grids. Field emission-scanning electron microscopy (FE-SEM) images were obtained with a ZEISS LEO 982 GEMINI field emission electron microscope using an in-lens detector to improve resolution.

Optical Characterization. UV−vis spectra were obtained employing a Hewlett-Packard 8453 spectrophotometer in transmission mode; films were deposited on microscope glass slides. The thickness and the optical constants $n(\lambda)$ and $k(\lambda)$ of MOTF or NP-MOTF were characterized by ellipsometry in a commercial SOPRA GES5 multispectral ellipsometer in microspot configuration; ellipsometry data was analyzed with Winelli II (Sopra). Film porosity was determined by spectrometric ellipsometry while varying the water vapor pressure in a controlled humidity chamber, according to Boissiere et al.[47]

RESULTS AND DISCUSSION

Ag Nanoparticle Synthesis in MOTF. The synthesis procedures used to load Ag NPs inside SiO_2 and TiO_2 MOTFs were presented in detail in previous works.[24,25] Here, we have extended the synthesis of infiltrated Ag NP to the case of ZrO_2 MOTF for which similar trends are obtained. Figure 1a shows the absorption spectrum of ZrO_2 film templated with a triblock copolymer nonionic surfactant (Pluronics F-127) deposited on glass and after 5, 15, and 120 min of reaction in the $AgNO_3$/HCHO mixture. As a result of the nucleation and growth of Ag NPs, a plasmon band develops as shown in Figure 1a. A clear trend is visible showing a progressive increase in the band intensity and a red-shift (from 440 to 480 nm). This can be qualitatively attributed to the increase in the number of particles, their size, and their plasmon interactions, as was demonstrated for Au@TiO_2 MOTF.[48] In order to obtain a quantitative view, the filling process in ZrO_2 and TiO_2 thin films has been followed using X-ray reflectivity (XRR) and energy dispersive X-ray scattering (EDX).[24,49] As time evolves, the fraction of Ag synthesized inside the pores increases, reaching a maximum pore filling of around 45% in the case of TiO_2 based films (Supporting Information Figure S2) and 25% in the case of ZrO_2 after 2h of reaction (Figure 1b).

Figure 2 shows TEM images of Ag@ZrO_2 MOTF composite films after 5 and 120 min of reaction. These films present mesostructures derived from cubic *Im3m* or *Fm3m* uniaxially

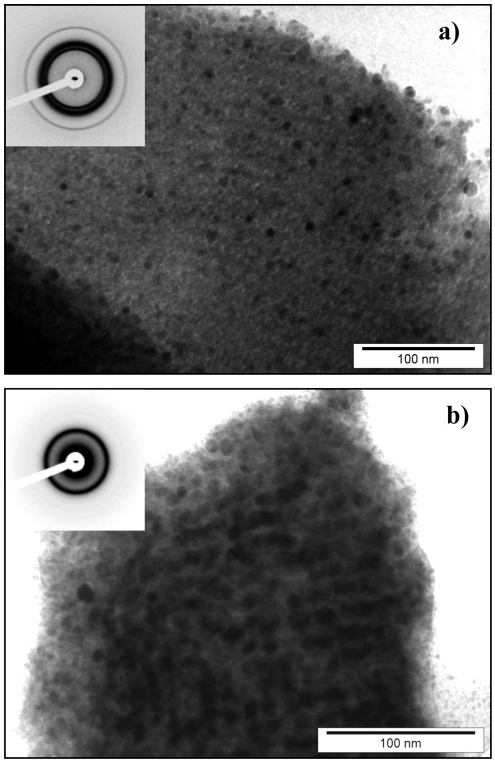

Figure 2. TEM micrographs of Ag@ZrO_2 mesoporous films at different Ag NP synthesis stages after: (a) 5 min and (b) 2 h.

dx.doi.org/10.1021/am500631f | ACS Appl. Mater. Interfaces 2014, 6, 5263−5272

distorted after thermal treatment according to SAXS and TEM. After $AgNO_3$ chemical reduction, uniform Ag particles are embedded within the ZrO_2 matrix pores, and are visualized as dark spots ~8−10 nm diameter, in good agreement with the known pore dimensions of F127-templated MOTF. The mesoporous host limits the Ag NPs size but not the distribution within the templated mesostructure. SAXS of samples after reduction, performed at 90° incidence show a diffraction ring corresponding to the d_{110} distance of an *Im3m* mesostructure located at 131 Å (a = 18.5 nm), pointing out that the mesopore structure remains intact after Ag synthesis (inset in Figure 2a).

When increasing the electroless deposition time (Figure 2b), a higher density of homogeneously distributed Ag NPs along the mesoporous matrix is observed. SAXS also shows that the mesoporous structure long-range is preserved when small doping of particles is analyzed. For longer reduction times, Ag loading within the mesopores becomes higher and two features are observed (insets in Figure 2a and b): a diffuse scattering due to the higher NPs content appears at low q values, and the intensity of the d_{110} diffraction signal decreases because of an increase in the average electronic density of the pores that decreases in turn the scattering contrast between pore and inorganic walls. Although the NPs are not forming an ordered array, a careful observation of the TEM data shows that they are homogeneously distributed along the MOTF samples.[24]

SERS Signal in Ag@ZrO_2 MOTF Matrices. After 4-MP (C_{2v} molecule) adsorption in the NP-MOTF films, Raman signals clearly show up in a series of spectra with different loading of Ag NPs (Figure 3a). For nanocomposite films produced after very short reduction times, no distinguishable features are observed and the spectra are characterized by a large background with broad features. For longer reduction times, the Ag NPs loading increases, and clear and intense Raman lines develop, accompanied by a steady decrease of the background. The bands around 1100 cm^{-1} and 1008 cm^{-1} are associated with the ring breathing and the C−S stretching mode of the molecule, while at 1210 cm^{-1} the characteristic $\beta_{(CH)}$ mode of 4-MP is observed.[50]

Figure 3b shows the intensity profile of the 1100 cm^{-1} Raman signal of 4-MP as a function of the laser excitation wavelength for the Ag@ZrO_2 substrates with increasing Ag loading time. The three Raman profiles display a maximum signal at around ~500 nm; a slight shift to longer wavelengths can be observed as the Ag NP filling increases. The wavelength interval of the signal increase agrees well with the plasmon resonance of isolated Ag nanoparticles (cf. the absorption spectra shown in Figure 1a). In addition, a Raman intensity tail toward longer wavelengths is also observed, which becomes a shoulder around ~550 nm as the Ag loading increases. This region of the spectrum is typical of plasmon modes due to interacting particles, as discussed in our previous work.[48,51−53] The observed correlation between the plasmon resonances and the increase of the observed signal strongly suggests that the confined Ag NPs are responsible of this Raman enhancement.

Raman Excitation Profiles for Different MOTFs. Figure 4 compares the Raman spectra for different SERS-active substrates. Nanocomposites Ag@TiO_2 and Ag@ZrO_2 matrices show almost the same spectra as a mechanically roughened Ag surface, with slightly lower intensities.

As previously mentioned, an important factor for the development of an analytical platform for SERS enhanced signals is the requisite to have a reproducible and spatially homogeneous signal.[3,10] In this work, a SERS signal was always observed when Ag NPs were synthesized inside the pores of different MOTFs. As shown in Figure 5, the dependence of the Raman intensity signal with laser excitation wavelength measured at 1100 cm^{-1} shows similar behavior for the MOTF studied but with peak location and broadness dependent on the mesoporous oxide matrix used.

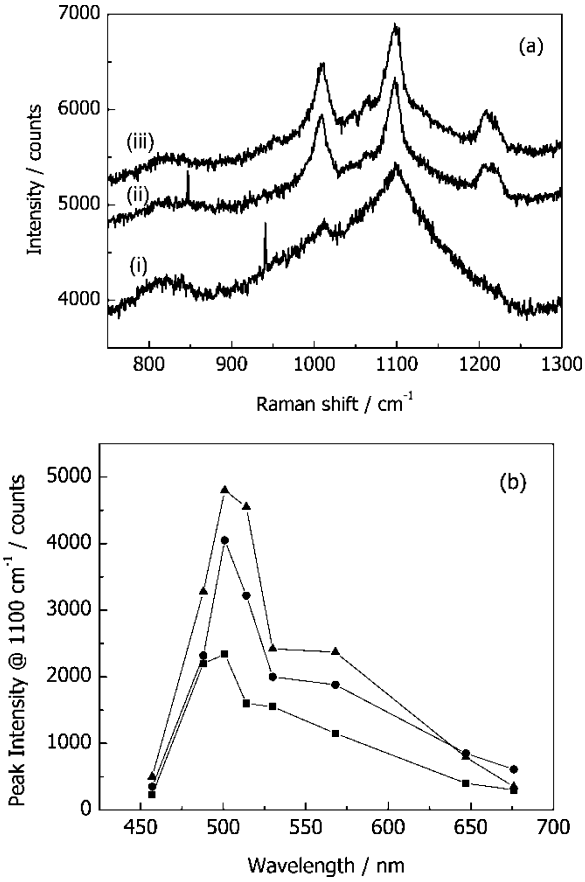

Figure 3. (a) 4-MP Raman spectra in Ag@ZrO_2 MOTF deposited on glass after $AgNO_3$/HCHO electroless deposition with increasing reaction times: (i) 5, (ii) 15, and (iii) 120 min. (b) Raman intensity profile of the 4-MP signal as a function of the laser excitation wavelength for the Ag@ZrO_2 MOTF after (■) 5, (●) 15, and (▲) 120 min of electroless deposition. Lines are for eye guidance only.

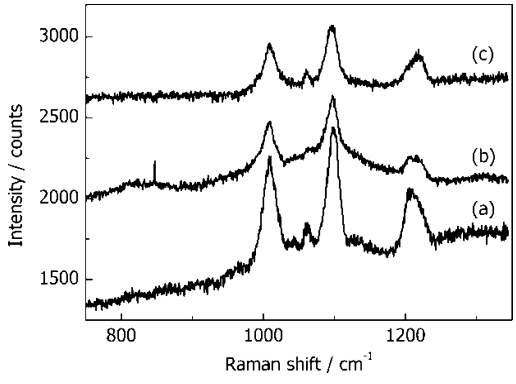

Figure 4. 4-MP Raman spectra measured over different systems (a) mechanically roughened Ag, (b) Ag@ZrO_2 MOTF, and (c) Ag@TiO_2 MOTF. The samples were excited with a laser at 568.1 nm with 10 mW output and 30 s of acquisition time. 4-MP was adsorbed from a 0.25 mM solution.

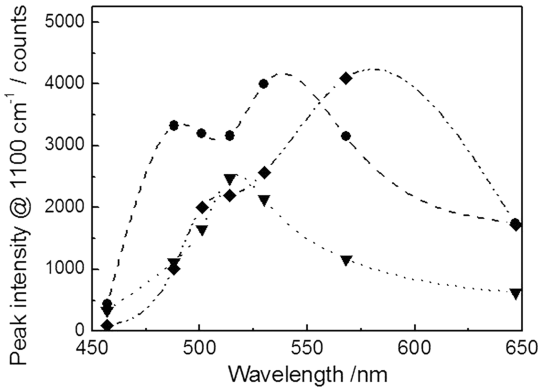

Figure 5. Raman intensity signal at 1100 cm^{-1} with variable wavelength laser excitation for different Ag@MOTF: (▼) Ag@ZrO_2, (◆) Ag@TiO_2, and (●) Ag@SiO_2. Lines are for eye guidance only.

Control experiments in empty MOTFs gave only background signals (see Supporting Information Figure S3) whereas metal NPs assembled over non mesoporous frameworks or Ag roughened foils gave highly nonuniform signals, as shown previously.[50]

SERS Signal Uniformity in Ag@MOTF. AgNP-MOTF matrices show a remarkably homogeneous spatial distribution of Raman intensities within 10% of signal dispersion in a 1 mm^2 area as shown in Figure 6 for various matrices. This is a promising result in terms of a reproducible platform for analytical determinations.[19] Recent work has reported 5−6% standard deviation in the pentachlorophenol SERS signal obtained on cysteamine-modified silver nanoparticle aggregates.[54] The route presented here permits to select among a choice of MOTF tailored for specific applications, or for further chemical surface pore modifications; detailed studies are underway.

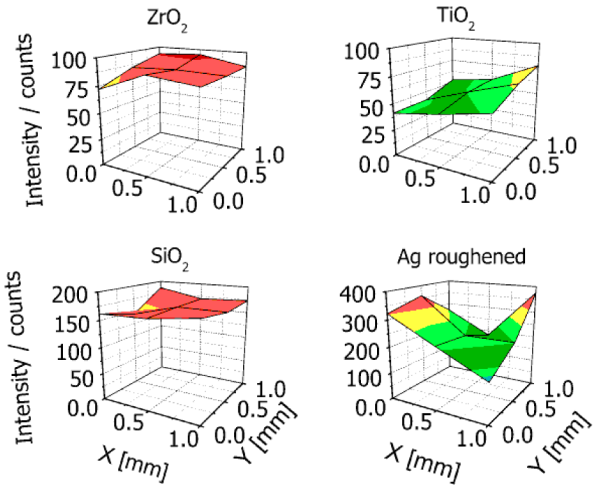

Figure 6. 1100 cm^{-1} 4-MP Raman signal maps of Ag@O_2 MOTF substrates studied in a 1 × 1 mm^2 area. Spots were measured every 0.5 mm using a 10 mW 514.5 nm laser line focused on a 100 μm circular spot. Acquisition time was 10 s. 1100 cm^{-1} signal averages are Ag@ZrO_2 (86 ± 6), Ag@TiO_2 (60 ± 10), SiO_2 (170 ± 10), and roughened Ag (260 ± 70).

As no signal is detected in the unloaded MOTFs, even after long acquisition times and higher 4-MP concentration, it was not possible to calculate an enhancement factor (EF); however, the similar intensity compared to Ag roughened substrates, which are typically characterized by EF on the order of 10^3−10^5, makes us estimate comparable values for our systems.[55,56] It is worth noting that the EISA approach presented here facilitates an easy substrate platform production and surface modification for SERS detection with the additional advantage of signal reproducibility. Other SERS substrates have been reported with higher enhancement factors but only after a sequence of complex steps or only on specific templates. In the following sections we will address the rational design of a TiO_2 MOTF platform that benefits from a photochemical strategy in order to localize the Ag NPs, and hence the Raman enhancement, and to generate uniform Raman spectra across the whole SERS surface substrate.

SERS Effect in TiO_2 MOTF with Photodeposited Ag NPs. Photodeposition of Ag NPs using UV photochemistry[57] opens the possibility to use conventional photolitography masks in order to transfer a pattern and therefore localize the regions of SERS enhancement. The photoreduction (PR) process for loading the mesoporous titania films with Ag NPs has some advantages compared to the electroless deposition method. For instance, the intensity of the UV light and the exposure time can be easily controlled. On the other hand, the stirring conditions during the electroless deposition method can have a significant effect in the homogeneity of the Ag NP loading, especially for large sample areas.

Ag NP synthesis within TiO_2 MOTF using the PR approach also results in homogeneously filled systems. Ellipsometric optical properties of the Ag@TiO_2 MOTF deposited on Si substrates are characterized by broad absorption spectra in the 500−700 nm range (see Supporting Information, Figure S5). Again, close contact between Ag NPs within the MOTF results in plasmon interactions affecting the observed spectra. Saturation filling fractions with Ag NPs obtained by this method (~55% of the total pore volume) are consistent with previous works.[25,45] Nonetheless, the PR approach is highly dependent on the photocatalytic properties of the TiO_2 anatase phase ($E_g \approx 3.2$ eV). The crystalline nature of the mesoporous film depends in turn on the film substrate and the thermal treatment applied.[58,59] The efficiency of Ag^+ photoreduction was found to be optimal (higher loading fraction at equal irradiation doses) when TiO_2 MOTFs are deposited on silicon instead of glass. The influence of the substrate on the PR method and the derived SERS effect is shown in the Supporting Information (Figure S4) where two kind of glasses, borosilicate (Pyrex) and soda-lime glass, were used in comparison with silicon. The photocatalytic nature of this method makes SiO_2 based MOTFs inert for this process. ZrO_2 MOTF display however a less efficient but noticeable Ag^+ photoreduction performance.

The SERS signals observed for PR processed NP-MOTF composites are intense and homogeneous along the substrates, as will be discussed in detail below in the case of 4-TP. Interestingly, when Rhodamine 6G and salicylic acid are put in contact with the SERS-active nanocomposite, intense SERS spectra are obtained, demonstrating that the molecules are in close proximity or even adsorbed onto the trapped Ag NPs, and can be detected (Supporting Information, Figure S6). Ongoing experiments are aimed at assessing whether these molecules are adsorbed onto the titania or the silver surface.

Patterning the SERS Effect. Figure 7 shows an example of the ability of the PR method to localize the SERS effect in an F127-templated TiO_2 MOTF deposited on silicon. The

dx.doi.org/10.1021/am500631f | ACS Appl. Mater. Interfaces 2014, 6, 5263−5272

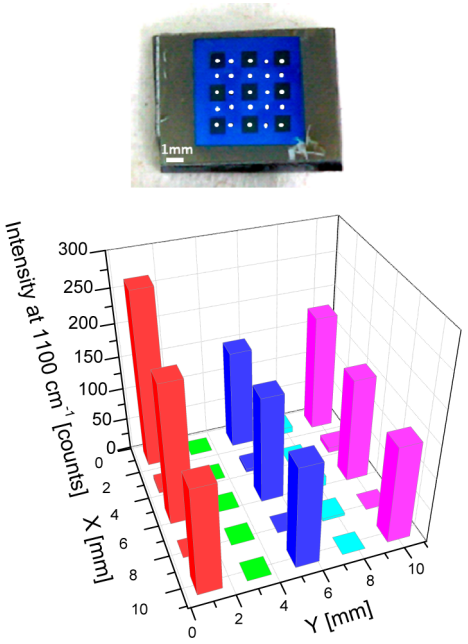

Figure 7. Raman intensity profile measured from the 4-MP peak intensity at 1100 cm^{-1} in F127-templated TiO_2 on silicon substrate, loaded with Ag NPs by PR method after 120 min of UV exposure with the use of a lithographic mask. Spectra obtained using 514.5 nm, 20 mW, 10 s. On top, optical image of the patterned sample showing in gray/blue the areas loaded/unloaded with Ag NPs; in white, the spots where the Raman spectrum of 4-MP was measured.

photolithography process was applied using an acetate mask with a pattern consisting in 1 mm side transparent squares, 1 mm spaced. The UV exposure time was 120 min, giving a filling fraction of (40 ± 5)% of the total porous volume of the film (45%). After the incubation of 4-MP the Raman signal was acquired in different points of the sample shown as white dots in the upper picture of Figure 7.

The intensity of the Raman signal, reported as the height in the main peak of 4-MP at 1100 cm^{-1}, is clearly dependent on the measurement spot, obtaining a noticeable Raman signal from the spots loaded with Ag. In addition, the spatial homogeneity of the Raman signal spans across the millimeter scale. The standard deviation of the signal homogeneity for the systems so far prepared is in the order of 20%, which can be attributed to the optics system used for the patterning (UV lamp and polymer masks), which are not yet optimized. However, Figure 7 shows the potential of NP-MOTF nanosystems to be integrated in lab-on-chip architectures that combine bottom−up with top−down strategies.

Substrate-to-substrate Raman signal repeatability is a fundamental issue that also needs to be satisfied in analytical methods.[19] Figure 8A shows the 4-MP Raman spectra of TiO_2 MOTF samples pertaining to independent synthesis batches. All samples were loaded with Ag NPs using the PR method with a 30 min UV exposure (metal filling fraction = 23 ± 3% of total porosity), then exposed to 4-MP and stored in the dark. The high reproducibility of the signals is evident (substrate-to-substrate standard deviation in the order of 10%), confirming that the method is highly reproducible and potentially scalable to real applications. When the nanocomposite substrates were stored in plastic bags under mild humidity and kept in the dark, the plasmonic properties did not change, and reproducible SERS signals could be obtained on substrates stored for periods of several months. This stability is greatly enhanced in the case of substrates exposed to thiol-containing analytes. Figure 8B shows the spectra of 4-MP loaded samples stored in the dark for periods up to 42 months. It can be observed that the signal variation is within 10% of the original signal, demonstrating that these NP-MOTF composites are extremely stable and can retain the analytes for long periods with no significant signal variations. This exceptional stability in the presence of thiol-containing molecules can be ascribed to a surface stabilization by thiol groups.

Ag Surface Particles on Ag@TiO_2 MOTF. In the electroless deposition and photodeposition methods reported here, it is possible to obtain highly controlled Ag NPs within the mesoporous matrix. However, depending on the synthesis or aging conditions, Ag NPs can be present at the surface of the porous oxide framework, which changes the SERS signal. As stated in the Experimental Section, a cleaning procedure is always applied after the synthesis of Ag NPs with any of the methods previously discussed. In this section we will analyze the influence of the surface deposited Ag NP particles on the SERS spectrum.

FE-SEM micrographs of different regions of the MOTF topmost surface after the photolithographic Ag NP synthesis

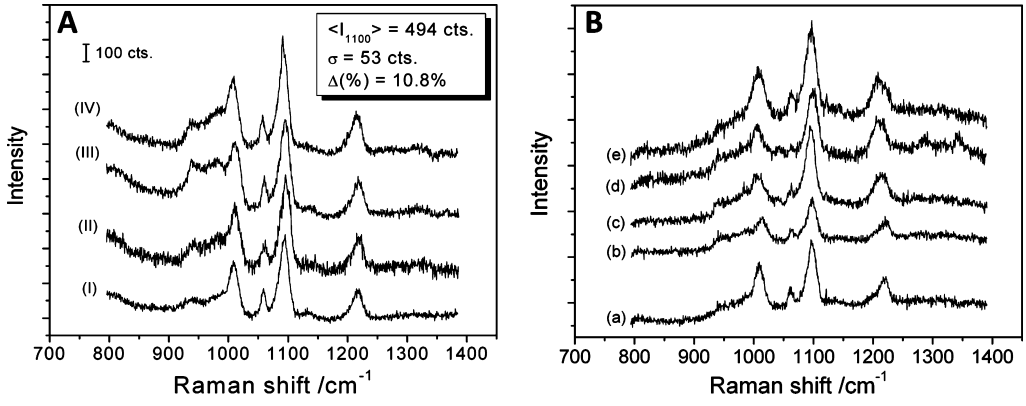

Figure 8. Raman spectra of 4-MP in Ag@TiO_2 MOTF/silicon loaded with Ag NPs by PR method after 30 min of UV exposure. (A) Measurements performed on different substrates, measured after preparation. (B) Measurements performed on independent substrates incubated with 4-MP prepared in different occasions. The elapsed time (in months) between preparation and measurement were (a) 0, (b) 1, (c) 5, (d) 23, and (e) 42 months.

dx.doi.org/10.1021/am500631f | ACS Appl. Mater. Interfaces 2014, 6, 5263−5272

are compared in Figure 9. As expected, right below the dark zones of the photolithographic mask, no Ag NPs on the

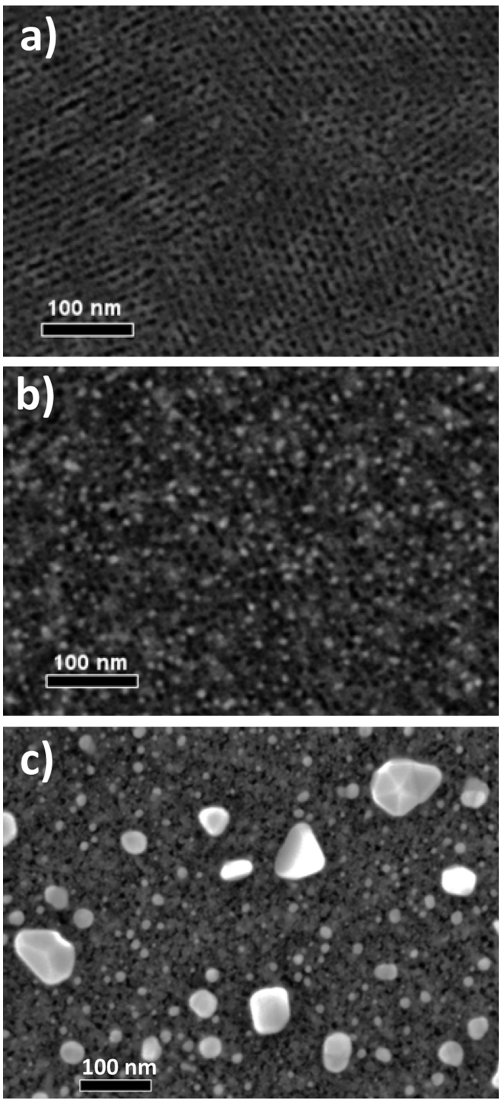

Figure 9. FE-SEM images of TiO_2−F127/silicon loaded with Ag by PR method using a phtolithography mask (t_{UV} = 30 min). (a) Surface state under the dark zone of the mask. (b) Surface under the transparent zone. (c) Surface in the uncovered region of the sample.

mesoporous film surfaces are detected (Figure 9a). On the other hand, in Figure 9b the TiO_2 surface under the transparent region of the mask shows a monodisperse distribution of Ag NPs with sizes comparable to the MOTF pore size (~10 nm). Clearly in Figure 9c, a different result is seen when no lithography mask is used. In that case, larger particles of irregular shapes (faceted, triangular plates and rods) and smaller particles in very close contact covering the MOTF surface are observed.

These Ag surface particles have an important influence on the Raman signal enhancement, as shown in Figure 10. In the absence of any photolithographic mask and no cleaning, where the surface of the MOTF is directly exposed to the silver precursor solution, very intense Raman signals are obtained (Figure 10a). However, the SERS effect strongly depends on the measurement location due to the inhomogeneous distribution of Ag particles and the resulting "hot spots" on

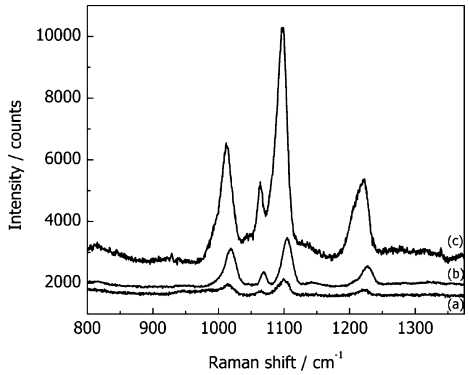

Figure 10. Raman spectra of 10 μM 4-MP adsorbed in Ag@TiO_2 MOTF/silicon by the PR method: (a) photolithographic mask and performing a surface cleaning, (b) photolithographic mask and no surface cleaning step, and (c) no photolithographic mask and no surface cleaning. In all cases, UV illumination time for Ag NP synthesis was 30 min. Laser excitation wavelength was 514.5 nm, 20 mW. Signal was acquired twice for 60 s and averaged.

the MOTF surface. In contrast, Raman enhancements in the regions that were exposed to UV light under the transparent regions of the mask are 3 to 5 times lower, whether or not the surface is cleaned (Figure 10b and c). Again, only after cleaning with a tissue paper, a reproducible although less intense spectrum is obtained across the Raman active film.

It is worth mentioning that although the intensity of the signal is almost 1 order of magnitude higher in the samples presenting surface nanoparticles than in the cleaned samples, those high signals are quite inhomogeneous throughout the film surface. Therefore, if an analytical technique is to be developed, there will be a trade-off between high signal intensity and reproducibility.[19] This effect has been recently reported in yolk-porous shell nanocomposite colloids, and an extra purification step was deemed as a necessary step toward a predictable functionality for SERS-active nanomaterials.[60]

SERS Effect in Bilayered Mesoporous Structures. A photochemically nonreactive SiO_2 mesoporous layer was deposited on top of a nanoparticle-loaded mesoporous titania thin film. Previous works demonstrated that Ag^+ can be selectively photoreduced within the TiO_2 layer in silica−titania bilayer MOTF, leading to vertical positioning of NP because of chemical selectivity.[25] With the addition of the photopatterning procedures, the extension to 3D localization is straightforward. The presence of a top mesoporous film with controllable pore size and surface chemistry would allow the diffusion of the SERS analyte while excluding the presence of superficial inhomogeneous hot spots and Ag NP, which is an important issue regarding the reproducibility of SERS measurements as demonstrated above. Apart from resolving the "particle on surface" problem by avoiding their formation, since no nucleation takes place on SiO_2, an empty mesoporous overlayer represents an opportunity for the control of the selectivity in analyte detection, as mesoporous SiO_2 MOTF (upper layer) can be tuned both in its pore size and its surface functionality, acting as porous permselective membranes (see Scheme 1).[25,26] Recently, López-Puente et. al demonstrated that mesoporous thin films can act as molecular sieves, allowing selective diffusion and detection of small molecules in biological mixtures.[20]

Figure 11 shows the Raman spectra of 4-MP on a bilayer structured sample comprising a SiO_2−CTAB layer (103 ± 4

dx.doi.org/10.1021/am500631f | ACS Appl. Mater. Interfaces 2014, 6, 5263−5272

Scheme 1. Schematic Representation of a Bilayered MOTF with a SiO_2 MOTF Templated with CTAB over a TiO_2 MOTF Templated with Pluronics F127[a]

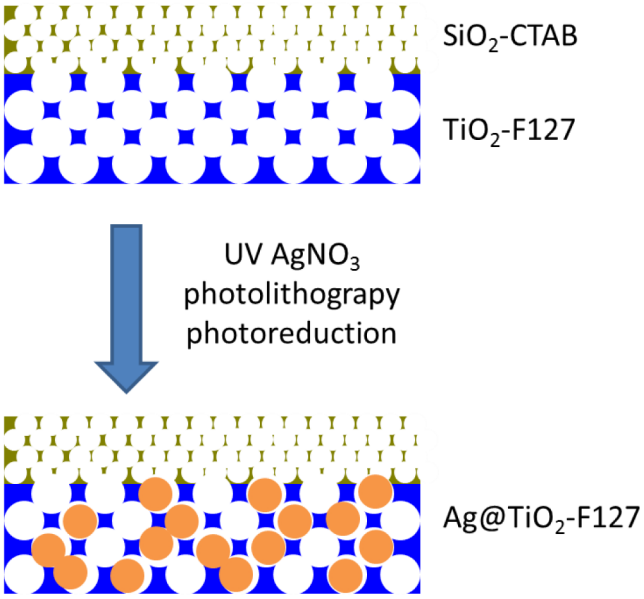

[a]Ag NP synthesis occurs only in the TiO_2 MOTF layer.

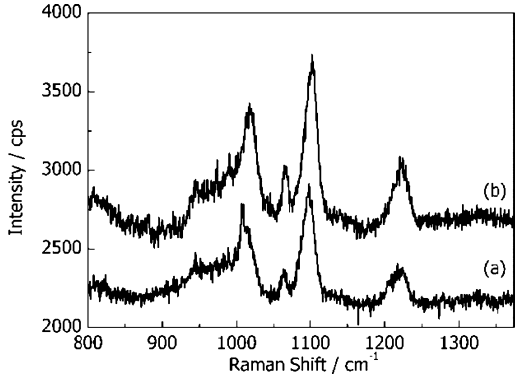

Figure 11. Raman spectra of 10 μM 4-MP adsorbed in (a) bilayer SiO_2−CTAB/Ag@TiO_2 MOTF/silicon and (b) Ag@TiO_2-MOTF/silicon. Both systems were loaded with Ag NPs using the PR method with a lithographic mask and 120 min of UV exposure. Laser excitation wavelength was 514.5 nm, 20 mW output power. Signal was acquired twice for 60 s and averaged.

nm thick) deposited over a TiO_2−F127 (110 ± 5 nm thick) and loaded with Ag NPs by PR after 120 min of UV exposure using a photolithographic mask.

In this kind of bilayer structures, the areas of the samples covered and uncovered with the photolithograpy mask display almost identical signal without any surface cleaning, showing the efficiency of the SiO_2 layer in avoiding Ag particle formation. This experiment demonstrates that the Ag NP embedded within the TiO_2 MOTF give rise to the Raman spectrum observed, even if they are "buried" in a multilayer.

CONCLUSIONS

In summary, we have demonstrated a reproducible and simple substrate platform based on mesoporous oxide thin films containing Ag NP for SERS chemical analysis. Reproducible Raman-active nanocomposite substrates have been obtained on TiO_2, SiO_2, and ZrO_2 MOTFs. Raman signals are well-defined and uniform in the submillimeter scale across centimeter-sized substrates. The different oxide frameworks are high *k*-dielectric, optically transparent and provide specific surface chemistries with characteristic properties: photocatalysis (TiO_2), tunable surface silane chemistry (SiO_2) and resistance to harsh chemical conditions (ZrO_2). It has been demonstrated that these MOTF can be modified by adding a wide variety of nanoparticulate, organic or polymeric modifiers.[61] This broad palette of metal NP supporting materials opens the possibility for specific SERS substrates with tailored properties and functions in an integrated chemical device. The modulation of the NP surface plasmon absorption using different MOTF matrices and pore sizes tunes SERS intensity and wavelength selectivity.[48] In addition, bilayer structures and photolithography provide additional freedom in the design of functional plasmon based sensors by locating the Ag loading.

The obtained SERS enhancements observed here are not spectacular, but we have to stress that they are extremely reproducible, that the NP-MOTF Raman signals are exceptionally stable along time, and that the substrates are easy to prepare through a highly reproducible and low-cost method that permits to process large surfaces. All these factors intervene in the overall performance of a nanostructured substrate.[19] The trend in current literature is to report exceptional enhancement factors, and the rest of the components of the performance vector are seldom analyzed. These often neglected factors are crucial in the case of real integrated biomolecule sensing systems, in which, apart from ultrahigh sensitivity, it is highly desirable to quantitatively assess the analyte concentration. This requires extremely reproducible SERS substrates, which can withstand repeated and reliable calibrations.[10] The approach presented here, based on low cost EISA dip coating methods, can be extended to surfaces of arbitrary shape, lab-on-chip setups, microfluidic channels and nanometric and colloidal probes.[62] In addition, there is still plenty of room to optimize the silver loading and interconnectivity, in order to tune the plasmons and hot spots within the mesopore system.[25,45,48] Given that the Raman signal is strongly dependent on the available Ag surface for binding 4-MP, the interconnected pores in the MOTF matrices have to fulfill a double purpose: on one hand, they provide the support for the Ag NPs, and on the other, they allow the free diffusion of analytes/reactants to reach the Ag surface. This results in a compromise between a high density of Ag metallic surfaces for anchoring 4-MP and keeping the interconnectivity in the system at maximum. Mesoporous systems have in addition the possibility to generate permselectivity, either by anchoring functional groups or polymers to the MOTF surface[63−65] or by using multilayers, resulting in a new generation of fully integrated chemical devices and microarray setups for complex problems such as environmental issues or proteomics.[66]

ASSOCIATED CONTENT

Supporting Information

Figures presenting structural analysis (XRR, UV−vis), Raman spectra of 4-MP adsorbed onto different substrates, of other analytes, and signals of blank experiments, are provided. This information is available free of charge via the Internet at http://pubs.acs.org/.

AUTHOR INFORMATION

Corresponding Author

*E-mail: gsoler@cnea.gov.ar. Fax: 54-11-6772-7886. Phone: 54-11-6772-7032.

Author Contributions

†A.W., N.G.T., and E.D.M. contributed equally to this work.

Notes

The authors declare no competing financial interest.

ACKNOWLEDGMENTS

Funding was provided by CONICET (PIP 5191), ANPCyT (PICT #0026, #33973, #1848, #2087 #00392, #2012-1167 PAE 2004 22711), UBACyT (20020100100636), UNSAM (SJ10/20), CONICET (GI-PIP 11220110101020) and ABT-Lus for access to LNLS SAXS1 and XRD2 beamlines. G.J.A.A.S.I, A.W., H.T., A.F., M.C.F, M.G., N.T., and S.A.B. are members of CONICET. E.D.M. acknowledges a doctoral fellowship from CONICET.

REFERENCES

(1) Fleischmann, M.; Hendra, P.; McQuillan, A. Raman spectra of pyridine adsorbed at a silver electrode. *Chem. Phys. Lett.* **1974**, *26* (2), 163−166.

(2) Nie, S.; Emory, S. R. Probing single molecules and single nanoparticles by surface-enhanced Raman scattering. *Science* **1997**, *275* (5303), 1102−1106.

(3) Baker, G. A.; Moore, D. S. Progress in plasmonic engineering of surface-enhanced Raman-scattering substrates toward ultra-trace analysis. *Anal. Bioanal. Chem.* **2005**, *382* (8), 1751−1770.

(4) Kneipp, K.; Wang, Y.; Kneipp, H.; Perelman, L. T.; Itzkan, I.; Dasari, R.; Feld, M. S. Single molecule detection using surface-enhanced Raman scattering (SERS). *Phys. Rev. Lett.* **1997**, *78* (9), 1667−1670.

(5) Moskovits, M. Surface-enhanced Raman spectroscopy: A brief retrospective. *J. Raman Spectrosc.* **2005**, *36* (6−7), 485−496.

(6) Etchegoin, P.; Maher, R. C.; Cohen, L. F.; Hartigan, H.; Brown, R. J. C.; Milton, M. J. T.; Gallop, J. C. New limits in ultrasensitive trace detection by surface enhanced Raman scattering (SERS). *Chem. Phys. Lett.* **2003**, *375* (1−2), 84−90.

(7) Jiang, J.; Bosnick, K.; Maillard, M.; Brus, L. Single molecule Raman spectroscopy at the junctions of large Ag nanocrystals. *J. Phys. Chem. B* **2003**, *107* (37), 9964−9972.

(8) Markel, V. A.; Shalaev, V. M.; Zhang, P.; Huynh, W.; Tay, L.; Haslett, T. L.; Moskovits, M. Near-field optical spectroscopy of individual surface-plasmon modes in colloid clusters. *Phys. Rev. B: Condens. Matter Mater. Phys.* **1999**, *59* (16), 10903−10909.

(9) Zayak, A. T.; Hu, Y. S.; Choo, H.; Bokor, J.; Cabrini, S.; Schuck, P. J.; Neaton, J. B. Chemical Raman enhancement of organic adsorbates on metal surfaces. *Phys. Rev. Lett.* **2011**, *106* (8), 083003−083006.

(10) Ko, H.; Singamaneni, S.; Tsukruk, V. V. Nanostructured surfaces and assemblies as SERS media. *Small* **2008**, *4* (10), 1576−1599.

(11) Jones, M. R.; Osberg, K. D.; Macfarlane, R. J.; Langille, M. R.; Mirkin, C. A. Templated techniques for the synthesis and assembly of plasmonic nanostructures. *Chem. Rev.* **2011**, *111* (6), 3736−3827.

(12) Brolo, A. G.; Arctander, E.; Gordon, R.; Leathem, B.; Kavanagh, K. L. Nanohole-enhanced raman scattering. *Nano Lett.* **2004**, *4* (10), 2015−2018.

(13) Jensen, T. R.; Schatz, G. C.; Van Duyne, R. P. Nanosphere lithography: Surface plasmon resonance spectrum of a periodic array of silver nanoparticles by ultraviolet−visible extinction spectroscopy and electrodynamic modeling. *J. Phys. Chem. B* **1999**, *103* (13), 2394−2401.

(14) Mahajan, S.; Abdelsalam, M.; Suguwara, Y.; Cintra, S.; Russell, A.; Baumberg, J.; Bartlett, P. Tuning plasmons on nano-structured substrates for NIR-SERS. *Phys. Chem. Chem. Phys.* **2007**, *9* (1), 104−109.

(15) Wang, H.; Levin, C. S.; Halas, N. J. Nanosphere arrays with controlled sub-10-nm gaps as surface-enhanced Raman spectroscopy substrates. *J. Am. Chem. Soc.* **2005**, *127* (43), 14992−14993.

(16) Lee, S. J.; Morrill, A. R.; Moskovits, M. Hot spots in silver nanowire bundles for surface-enhanced Raman spectroscopy. *J. Am. Chem. Soc.* **2006**, *128* (7), 2200−2201.

(17) Wu, Y.; Livneh, T.; Zhang, Y. X.; Cheng, G.; Wang, J.; Tang, J.; Moskovits, M.; Stucky, G. D. Templated synthesis of highly ordered mesostructured nanowires and nanowire arrays. *Nano Lett.* **2004**, *4* (12), 2337−2342.

(18) Wang, X.; Li, M.; Meng, L.; Lin, K.; Feng, J.; Huang, T.; Yang, Z.; Ren, B. Probing the location of hot spots by surface-enhanced Raman spectroscopy: Toward uniform substrates. *ACS Nano* **2014**, *8* (1), 528−536.

(19) Brown, R. J. C.; Milton, M. J. T. Nanostructures and nanostructured substrates for surface-enhanced Raman scattering (SERS). *J. Raman Spectrosc.* **2008**, *39* (10), 1313−1326.

(20) López-Puente, V.; Abalde-Cela, S.; Angelomé, P. C.; Alvarez-Puebla, R. A.; Liz-Marzán, L. M. Plasmonic mesoporous composites as molecular sieves for SERS detection. *J. Phys. Chem. Lett.* **2013**, *4* (16), 2715−2720.

(21) Malfatti, L.; Falcaro, P.; Marmiroli, B.; Amenitsch, H.; Piccinini, M.; Falqui, A.; Innocenzi, P. Nanocomposite mesoporous ordered films for lab-on-chip intrinsic surface enhanced Raman scattering detection. *Nanoscale* **2011**, *3* (9), 3760−3766.

(22) Mura, S.; Greppi, G.; Innocenzi, P.; Piccinini, M.; Figus, C.; Marongiu, M. L.; Guo, C.; Irudayaraj, J. Nanostructured thin films as surface-enhanced Raman scattering substrates. *J. Raman Spectrosc.* **2013**, *44* (1), 35−40.

(23) Sugikawa, K.; Nagata, S.; Furukawa, Y.; Kokado, K.; Sada, K. Stable and functional gold nanorod composites with a metal−organic framework crystalline shell. *Chem. Mater.* **2013**, *25* (13), 2565−2570.

(24) Fuertes, M. C.; Marchena, M.; Marchi, M. C.; Wolosiuk, A.; Soler-Illia, G. J. A. A. Controlled deposition of silver nanoparticles in mesoporous single- or multilayer thin films: From tuned pore filling to selective spatial location of nanometric objects. *Small* **2009**, *5* (2), 272−280.

(25) Martínez, E. D.; Granja, L.; Bellino, M. G.; Soler-Illia, G. J. A. A. Electrical conductivity in patterned silver-mesoporous titania nanocomposite thin films: Towards robust 3D nano-electrodes. *Phys. Chem. Chem. Phys.* **2010**, *12* (43), 14445−14448.

(26) Soler-Illia, G. J. D. A. A.; Sanchez, C.; Lebeau, B.; Patarin, J. Chemical strategies to design textured materials: From microporous and mesoporous oxides to nanonetworks and hierarchical structures. *Chem. Rev.* **2002**, *102* (11), 4093−4138.

(27) Yamauchi, Y.; Momma, T.; Kitoh, H.; Osaka, T.; Kuroda, K. Fabrication of mesoporous Pt inside micrometer channels via "solvent-evaporation-mediated direct physical casting". *Electrochem. Commun.* **2005**, *7* (12), 1364−1370.

(28) Yang, P.; Deng, T.; Zhao, D.; Feng, P.; Pine, D.; Chmelka, B. F.; Whitesides, G. M.; Stucky, G. D. Hierarchically ordered oxides. *Science* **1998**, *282* (5397), 2244−2246.

(29) Fuertes, M. C.; Colodrero, S.; Lozano, G.; González-Elipe, A. R.; Grosso, D.; Boissière, C.; Sánchez, C.; Soler-Illia, G. J. D. A. A.; Míguez, H. Sorption properties of mesoporous multilayer thin films. *J. Phys. Chem. C* **2008**, *112* (9), 3157−3163.

(30) Yang, P.; Rizvi, A. H.; Messer, B.; Chmelka, B. F.; Whitesides, G. M.; Stucky, G. D. Patterning porous oxides within microchannel networks. *Adv. Mater.* **2001**, *13* (6), 427−431.

(31) Calvo, A.; Angelomé, P. C.; Sánchez, V. M.; Scherlis, D. A.; Williams, F. J.; Soler-Illia, G. J. A. A. Mesoporous aminopropyl-functionalized hybrid thin films with modulable surface and environment-responsive behavior. *Chem. Mater.* **2008**, *20* (14), 4661−4668.

(32) Calvo, A.; Yameen, B.; Williams, F. J.; Azzaroni, O.; Soler-Illia, G. J. A. A. Facile molecular design of hybrid functional assemblies with controllable transport properties: Mesoporous films meet polyelectrolyte brushes. *Chem. Commun.* **2009**, *18*, 2553−2555.

(33) Angelomé, P. C.; Cecilia Fuertes, M.; Soler-Illia, G. J. A. A. Multifunctional, multilayer, multiscale: Integrative synthesis of complex macroporous and mesoporous thin films with spatial separation of porosity and function. *Adv. Mater.* **2006**, *18* (18), 2397−2402.
(34) Fuertes, M. C.; López-Alcaraz, F. J.; Marchi, M. C.; Troiani, H. E.; Luca, V.; Míguez, H.; Soler-Illia, G. J. D. A. A. Photonic crystals from ordered mesoporous thin-film functional building blocks. *Adv. Funct. Mater.* **2007**, *17* (8), 1247−1254.
(35) Zelcer, A.; Wolosiuk, A.; Soler-Illia, G. J. A. A. Carbonaceous submicron sized islands: A surface patterning route to hierarchical macro/mesoporous thin films. *J. Mater. Chem.* **2009**, *19* (24), 4191−4196.
(36) Crepaldi, E. L.; Soler-Illia, G. J. D. A. A.; Grosso, D.; Cagnol, F.; Ribot, F.; Sanchez, C. Controlled formation of highly organized mesoporous titania thin films: From mesostructured hybrids to mesoporous nanoanatase TiO_2. *J. Am. Chem. Soc.* **2003**, *125* (32), 9770−9786.
(37) Sanchez, C.; Boissière, C.; Grosso, D.; Laberty, C.; Nicole, L. Design, synthesis, and properties of inorganic and hybrid thin films having periodically organized nanoporosity. *Chem. Mater.* **2008**, *20* (3), 682−737.
(38) Attard, G. S.; Bartlett, P. N.; Coleman, N. R. B.; Elliott, J. M.; Owen, J. R.; Wang, J. H. Mesoporous platinum films from lyotropic liquid crystalline phases. *Science* **1997**, *278* (5339), 838−840.
(39) Pérez, M. D.; Otal, E.; Bilmes, S. A.; Soler-Illia, G. J. A. A.; Crepaldi, E. L.; Grosso, D.; Sanchez, C. Growth of gold nanoparticle arrays in TiO_2 mesoporous matrixes. *Langmuir* **2004**, *20* (16), 6879−6886.
(40) Besson, S.; Gacoin, T.; Ricolleau, C.; Boilot, J. P. Silver nanoparticle growth in 3D-hexagonal mesoporous silica films. *Chem. Commun.* **2003**, *9* (3), 360−361.
(41) Huang, M. H.; Choudrey, A.; Yang, P. Ag nanowire formation within mesoporous silica. *Chem. Commun.* **2000**, *12*, 1063−1064.
(42) Kumai, Y.; Tsukada, H.; Akimoto, Y.; Sugimoto, N.; Seno, Y.; Fukuoka, A.; Ichikawa, M.; Inagaki, S. Highly ordered platinum nanodot arrays with cubic symmetry in mesoporous thin films. *Adv. Mater.* **2006**, *18* (6), 760−762.
(43) Wright, A.; Gabaldon, J.; Burckel, D. B.; Jiang, Y. B.; Tian, Z. R.; Liu, J.; Brinker, C. J.; Fan, H. Hierarchically organized nanoparticle mesostructure arrays formed through hydrothermal self-assembly. *Chem. Mater.* **2006**, *18* (13), 3034−3038.
(44) Bronstein, L. Nanoparticles made in mesoporous solids. In *Colloid Chemistry I*; Antonietti, M., Ed.; Springer: Berlin, 2003; Chapter 3, pp 55−89.
(45) Martínez, E. D.; Bellino, M. G.; Soler-Illia, G. J. A. A. Patterned production of silver-mesoporous titania nanocomposite thin films using lithography-assisted metal reduction. *ACS Appl. Mater. Interfaces* **2009**, *1* (4), 746−749.
(46) Koura, N. Electroless plating of silver. In *Electroless Plating: Fundamentals and Applications*; Mallory, G. O., Hajdu, J. B., Eds.; American Electroplaters and Surface Finishers Society: Orlando, FL, 1990; Chapter 17, pp 441−462.
(47) Boissiere, C.; Grosso, D.; Lepoutre, S.; Nicole, L.; Bruneau, A. B.; Sanchez, C. Porosity and mechanical properties of mesoporous thin films assessed by environmental ellipsometric porosimetry. *Langmuir* **2005**, *21* (26), 12362−71.
(48) Sánchez, V. M.; Martínez, E. D.; Martínez Ricci, M. L.; Troiani, H.; Soler-Illia, G. J. A. A. Optical properties of Au nanoparticles included in mesoporous TiO_2 thin films: A dual experimental and modeling study. *J. Phys. Chem. C* **2013**, *117* (14), 7246−7259.
(49) Gibaud, A.; Dourdain, S.; Vignaud, G. Analysis of mesoporous thin films by X-ray reflectivity, optical reflectivity and grazing incidence small angle X-ray scattering. *Appl. Surf. Sci.* **2006**, *253* (1), 3−11.
(50) Baldwin, J. A.; Vlčková, B.; Andrews, M. P.; Butler, I. S. Surface-enhanced raman scattering of mercaptopyridines and pyrazinamide incorporated in silver colloid-adsorbate films. *Langmuir* **1997**, *13* (14), 3744−3751.
(51) Tognalli, N.; Fainstein, A.; Calvo, E.; Bonazzola, C.; Pietrasanta, L.; Campoy-Quiles, M.; Etchegoin, P. SERS in PAH-Os and gold nanoparticle self-assembled multilayers. *J. Chem. Phys.* **2005**, *123* (4), No. 044707.
(52) Jain, P. K.; El-Sayed, M. A. Plasmonic coupling in noble metal nanostructures. *Chem. Phys. Lett.* **2010**, *487* (4−6), 153−164.
(53) Ung, T.; Liz-Marzán, L. M.; Mulvaney, P. Optical properties of thin films of AuO/SiO_2 particles. *J. Phys. Chem. B* **2001**, *105* (17), 3441−3452.
(54) Jiang, X.; Yang, M.; Meng, Y.; Jiang, W.; Zhan, J. Cysteamine-modified silver nanoparticle aggregates for quantitative SERS sensing of pentachlorophenol with a portable Raman spectrometer. *ACS Appl. Mater. Interfaces* **2013**, *5* (15), 6902−8.
(55) Norrod, K. L.; Sudnik, L. M.; Rousell, D.; Rowlen, K. L. Quantitative comparison of five SERS substrates: Sensitivity and limit of detection. *Appl. Spectrosc.* **1997**, *51* (7), 994−1001.
(56) Sudnik, L. M.; Norrod, K. L.; Rowlen, K. L. SERS-active Ag films from photoreduction of Ag+ on TiO_2. *Appl. Spectrosc.* **1996**, *50* (3), 422−424.
(57) Henglein, A. Colloidal silver nanoparticles: Photochemical preparation and interaction with O_2, CCl_4, and some metal ions. *Chem. Mater.* **1998**, *10* (1), 444−450.
(58) Angelomé, P. C.; Andrini, L.; Calvo, M. E.; Requejo, F. G.; Bilmes, S. A.; Soler-Illia, G. J. A. A. Mesoporous anatase TiO_2 films: Use of Ti K XANES for the quantification of the nanocrystalline character and substrate effects in the photocatalysis behavior. *J. Phys. Chem. C* **2007**, *111* (29), 10886−10893.
(59) Yu, J.; Zhao, X. Effect of substrates on the photocatalytic activity of nanometer TiO_2 thin films. *Mater. Res. Bull.* **2000**, *35* (8), 1293−1301.
(60) Pierre, M. C. S.; Haes, A. J. Purification implications on SERS activity of silica coated gold nanospheres. *Anal. Chem.* **2012**, *84* (18), 7906−7911.
(61) Soler-Illia, G. J. A. A.; Angelome, P. C.; Fuertes, M. C.; Calvo, A.; Wolosiuk, A.; Zelcer, A.; Bellino, M. G.; Martinez, E. D. Mesoporous hybrid and nanocomposite thin films. A sol−gel toolbox to create nanoconfined systems with localized chemical properties. *J. Sol−Gel Sci. Technol.* **2012**, *57* (3), 299−312.
(62) Scodeller, P.; Flexer, V.; Szamocki, R.; Calvo, E. J.; Tognalli, N.; Troiani, H.; Fainstein, A. Wired-enzyme core-shell Au nanoparticle biosensor. *J. Am. Chem. Soc.* **2008**, *130* (38), 12690−12697.
(63) Calvo, A.; Yameen, B.; Williams, F. J.; Soler-Illia, G. J. A. A.; Azzaroni, O. Mesoporous films and polymer brushes helping each other to modulate ionic transport in nanoconfined environments. An interesting example of synergism in functional hybrid assemblies. *J. Am. Chem. Soc.* **2009**, *131* (31), 10866−10868.
(64) Fattakhova-Rohlfing, D.; Wark, M.; Rathouský, J. Ion-permselective pH-switchable mesoporous silica thin layers. *Chem. Mater.* **2007**, *19* (7), 1640−1647.
(65) Taffa, D. H.; Kathiresan, M.; Walder, L.; Seelandt, B.; Wark, M. Pore size and surface charge control in mesoporous TiO_2 using post-grafted SAMs. *Phys. Chem. Chem. Phys.* **2010**, *12* (7), 1473−1482.
(66) Mahajan, S.; Richardson, J.; Brown, T.; Bartlett, P. N. SERS-melting: A new method for discriminating mutations in DNA sequences. *J. Am. Chem. Soc.* **2008**, *130* (46), 15589−15601.